npj | Climate and Atmospheric Science

www.nature.com/npjclimatsci

ARTICLE OPEN

Check for updates

Investigating the impact of cloud-radiative feedbacks on tropical precipitation extremes

Brian Medeiros[1]✉, Amy C. Clement[2], James J. Benedict[2,3] and Bosong Zhang[2]

Although societally important, extreme precipitation is difficult to represent in climate models. This study shows one robust aspect of extreme precipitation across models: extreme precipitation over tropical oceans is strengthened through a positive feedback with cloud-radiative effects. This connection is shown for a multi-model ensemble with experiments that make clouds transparent to longwave radiation. In all cases, tropical extreme precipitation reduces without cloud-radiative effects. Qualitatively similar results are presented for one model using the cloud-locking method to remove cloud feedbacks. The reduced extreme precipitation without cloud-radiative feedbacks does not arise from changes in the mean climate. Rather, evidence is presented that cloud-radiative feedbacks enhance organization of convection and most extreme precipitation over tropical oceans occurs within organized systems. This result suggests that climate models must correctly predict cloud structure and properties, as well as capture the essence of organized convection in order to accurately represent extreme rainfall.

npj Climate and Atmospheric Science (2021)4:18 ; https://doi.org/10.1038/s41612-021-00174-x

INTRODUCTION

Cloud-radiative effects (CREs) are defined by the difference between the all-sky radiation flux and the clear-sky flux, and can be divided into shortwave (SW) and longwave (LW) components. Through CRE, clouds exert a strong and fundamental influence on the global mean climate. This influence is typically summarized using top-of-atmosphere (TOA) irradiance, where SWCRE dominates over LWCRE to produce a net cooling of ~18 W m^{-2}[1]. Clouds also influence surface irradiance, impacting the surface energy budget[2]. Within the atmospheric column, the difference between clear-sky and all-sky radiation fluxes, equivalent to the difference between the TOA and surface CRE and therefore a flux divergence, provides the atmospheric CRE (ACRE)[3–5]. The ACRE, along with latent heat release, directly couples clouds to the atmospheric flow, and numerous studies have pointed to LW effects, especially from upper-troposphere clouds, as a key influence of clouds on the circulation[6].

A spate of recent studies has shown that CREs also impact aspects of climate variability. Timescales from decadal[7,8] to interannual[9,10] to subseasonal[11,12] have all been studied. At the shorter timescales, emphasis has been given to the potential role of cloud-radiative feedbacks on the maintenance of the Madden–Julian oscillation (MJO) in the Indo-Pacific[13]. Other forms of organized convection have also been shown to depend on cloud-radiative feedbacks, including tropical cyclones[14–16].

The clouds that are most closely connected to organized tropical convection—and thereby the larger-scale circulation—are directly associated with deep convection. Experiments with cloud-resolving models (CRMs) configured in idealized radiative-convective equilibrium (RCE) show that the radiative effects of deep convective anvil clouds interact with the flow and help to reinforce circulations that connect moist convective regions to dry subsiding regions[17,18]. In experiments that interrupt the interaction between CRE and the flow (by making the clouds radiatively inactive), convection becomes more homogeneous across the domain. Recent experiments[18] show that two mechanisms compete: cloud-top radiative cooling destabilizes the column, while cloud-radiative heating stabilizes the column. With a large computational domain, however, the presence of the large-scale circulation mutes the influence of CRE on TOA radiation fluxes and cloud cover. At the resolved scales of CRMs (tens of km), these feedbacks between CRE and the flow appear to support self-organization of convection (aka aggregation) that is well documented in CRMs[19].

Climate models have lately been adapted for RCE experiments, and show similar convective organization (although on larger scales) as the high-resolution models[20–22]. Some of these studies have pointed to different mechanisms of convective aggregation than the CRM studies; for example, Coppin and Bony[23] show how low-level cloud effects drive aggregation at cooler surface temperatures. That study also showed that removing CRE stopped aggregation of convection, but, unlike others[17], showed that both low-level CRE and upper-level CRE can separately inhibit aggregation.

The aggregated convection in idealized modeling studies is usually thought to be closely related to real-world forms of organized convection, such as mesoscale convective systems (MCSs), tropical cyclones, and equatorial waves[19,24]. Aggregated or organized convection (using the terms synonymously) is associated with consolidated regions of deep clouds and ascending motion surrounded by clear skies and subsidence. In observations, such systems are easily found in geostationary satellite imagery, and cover a range of spatial scales[25–27]. When classified as MCSs, these regions of aggregated convection account for around half of tropical precipitation[28,29].

Although they are fairly common, organized convective events cover a small fraction of the tropical area, yet they account for a sizable proportion of precipitation. Therefore, the precipitation in organized convective events must be relatively intense. This deduction is supported by observations[30,31]. Outside the tropics, mesoscale systems are also a source of extreme precipitation[32]. In climate model projections, the extratropical extreme precipitation

[1]National Center for Atmospheric Research, Climate and Global Dynamics, Boulder, CO, USA. [2]Rosenstiel School of Marine and Atmospheric Science, University of Miami, Miami, FL, USA. [3]Los Alamos National Laboratory, Fluid Dynamics and Solid Mechanics, Los Alamos, NM, USA. ✉email: brianpm@ucar.edu

tends to increase with warming ~5–6% K^{-1}, but the tropics show less agreement[33], signaling a source of uncertainty in the projections.

Pendergrass et al.[34] used one climate model configured in RCE to examine how convective organization and extreme precipitation change with the climatic state. They showed that while the global mean precipitation smoothly increased with temperature, the degree of organization varied nonlinearly with prescribed surface temperature. The extreme precipitation was more closely connected to the degree of organization than the temperature. That study demonstrated that even a coarse-resolution climate model that does not resolve mesoscale circulations still produces organized convection, and the model's precipitation is more extreme when convection is more organized.

A chain of relationships begins to emerge from the current body of work on convective aggregation, extreme precipitation, and cloud-radiative feedbacks. Convective aggregation depends—at least to some degree—on cloud-radiative feedbacks, as demonstrated using CRMs[17,18]. Convective aggregation is thought to be closely related to observed forms of organized convection, such as moisture modes like the MJO and tropical depressions[26,27]. Recent work has also shown that in climate models, CREs impact aspects of organized convection[12] and that the representation of extreme precipitation depends on the degree of convective organization[34]. If CREs influence the convective organization, and if the convective organization is thought to be connected to extreme precipitation, it seems natural to ask how cloud-radiative feedbacks influence extreme precipitation.

Addressing that question is the focus of this study. We employ a hierarchy of climate model experiments that directly alter the representation of CRE. First, we investigate experiments in which clouds are radiatively inactive; this style of experiments has come to be referred to as COOKIE (Clouds On/Off Klima Intercomparison Experiment)[6,35,36]. Second, we compare the results from COOKIE experiments to experiments with one model in which cloud-radiation feedbacks are deactivated in such a way as to preserve the mean state, providing an alternative perspective on the impact of clouds on extreme precipitation. As will be shown, cloud-radiation feedbacks appear to enhance precipitation extremes, and we provide analysis supporting the notion that extreme precipitation sensitivity is related to aspects of organized convection.

RESULTS

Removing CREs

We analyze the COOKIE simulations contributed to the CMIP6 archive in two different configurations: standard Earth-like configurations (AMIP) and idealized aquaplanets. These simulations, contributed as part of the Cloud-Feedback Model Intercomparison Project (CFMIP)[37], have been conducted by five modeling groups at this time (four include aquaplanet experiments), and are listed in Table 1. The experimental protocol requests only LWCRE to be deactivated, so we refer to these as LWoff simulations. Sea-surface temperature and sea ice are prescribed and are identical between the control and LWoff simulations.

The only difference between control and LWoff simulations is that the clouds do not interact with LW radiation in LWoff. This is achieved by replacing the LW flux with the clear-sky LW flux (or equivalent operation, such as providing zero cloud fraction or optical depth to the radiation scheme). The advantage of modifying only the LW radiation is that surface warming associated with increased SW flux is avoided[6], reducing the impact of changes in the land-sea contrast that are not associated with coupling between clouds and circulation.

Table 1. Global mean precipitation change and energy budget components.

Model (abbrev.)	Case	δP	δE	δR_t	δR_b	δH	$\widetilde{\delta P}$
CESM2 (CESM2)	Aqua	−13.1	−13.1	−12.6	23.8	2.2	−13.4
	AMIP	−3.6	−3.7	−12.7	17.0	−0.6	−3.8
CNRM-CM6-1 (CNRM)	Aqua	−6.9	−6.9	−15.2	22.8	−0.6	−6.9
	AMIP	−4.4	−4.4	−15.5	19.8	0.1	−4.4
HadGEM3-GC31-LL (HadGEM3)	Aqua	−6.3	−6.3	−19.2	25.5	0.2	−6.6
	AMIP	−3.2	−3.3	−13.1	17.2	−0.8	−3.4
IPSL-CM6A-LR (IPSL)	Aqua	−8.5	−8.7	−13.9	24.1	−1.3	−8.8
	AMIP	−4.2	−4.3	−12.5	18.2	−1.4	−4.3
MRI-ESM2-0 (MRI)	AMIP	−3.4	−3.5	−15.9	21.2	−1.7	−3.5

All quantities are given as LWoff minus control, in units of W m^{-2}. The last column shows the estimated change in precipitation, $L_v\delta P = -\delta R_t - \delta R_b - \delta H$ (the L_v has been neglected in the column headings).

Figure 1 shows the zonal mean precipitation from the CFMIP LWoff experiments. The idealized aquaplanet simulations shown in Fig. 1a, b show the realistic AMIP configurations forced by monthly observed SST. The AMIP experiments show only modest changes in the zonal mean precipitation, but some changes are notable, such as the reduction in precipitation in the southern ocean stormtrack ~50°S and increased precipitation in the southern tropics. These changes are similar to results from a super-parameterized global atmospheric model in a similar experiment, where the changes were associated with changes in the ITCZ and Hadley circulation[38]. The aquaplanet configurations show more dramatic changes, with the tropical rain belts having reduced precipitation maxima in all four models as well as reduced precipitation in the midlatitude storm tracks. This exaggerated response in the aquaplanets suggests that cloud-radiation interactions drive feedbacks that, in the highly symmetric aquaplanet environment, strongly impact the hydrologic cycle and the circulation. The AMIP experiments contain additional variability due to seasonality and land-sea contrasts that are absent in the aquaplanets. The weakening and widening of the rain belts when CRE is deactivated is similar in experiments with both SW and LW effects removed[38,39].

There are energetic constraints on global average precipitation and its response to climate perturbations[40–42]. When taking a sufficiently long temporal average in a stable climate, the surface evaporation equals the precipitation. The atmospheric energy budget can be written as $\dot{\mathcal{E}}_a = R_t + R_b + L_vE + H$, where global and time averages are implied and $\mathcal{E}_a$ is the energy of the atmosphere (and the dot represents the total derivative), R_t is the TOA net radiation flux, R_b is the net surface radiation flux, L_v is the latent heat of vaporization of water, E is surface evaporative flux of water, and H is the surface-sensible heat flux[43]. Given a stable climate, $\mathcal{E}_a$ is invariant and $E = P$. This relates the global mean precipitation to the energy budget. Taking a difference between two climates, here the climates with and without cloud-radiation feedbacks, gives an expression for the change in global mean precipitation: $L_v\delta P = -\delta R_t - \delta R_b - \delta H$. This constraint is obeyed in coupled climate model experiments[5], but when the sea-surface temperature is prescribed as in AMIP and aquaplanet experiments, the surface energy budget does not necessarily balance[42]. Nonetheless, to a fair approximation, all the experiments examined here show the expected reduction in global mean precipitation given the change in the energy budget (Table 1). The change in surface-sensible heat flux is small compared to the changes in radiation fluxes. In LWoff

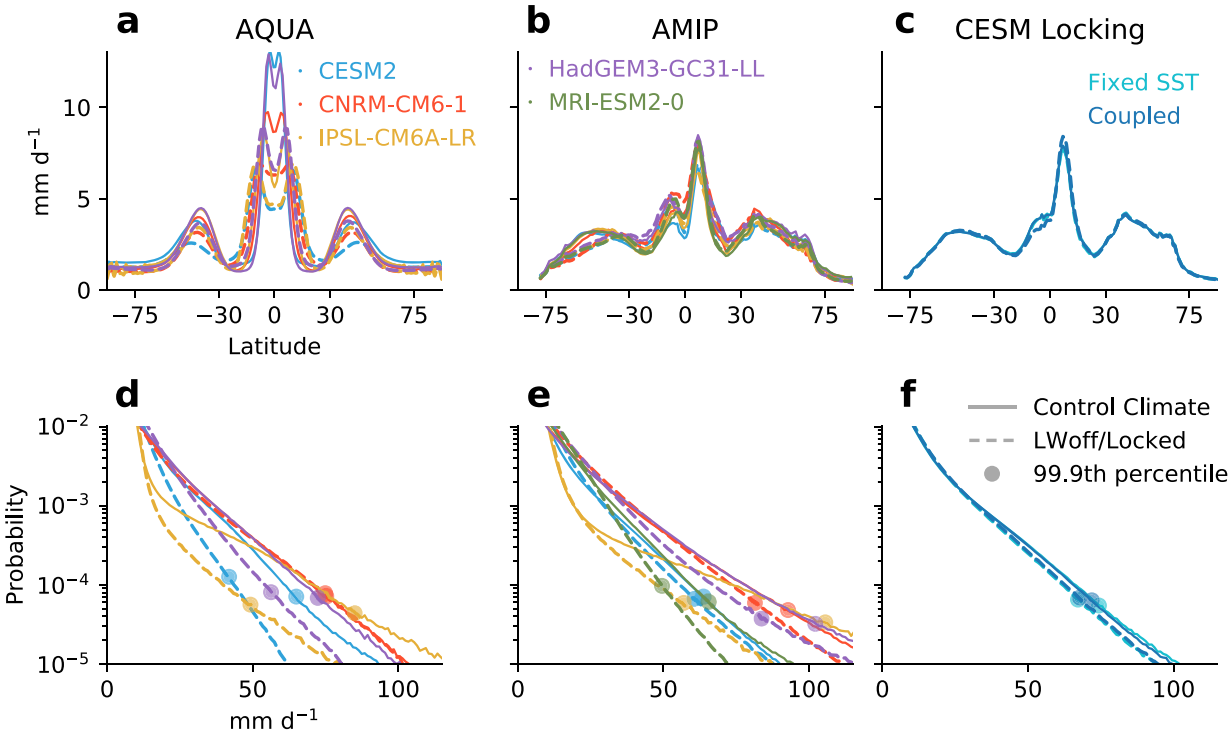

Fig. 1 Simulated precipitation distributions. a–c Zonal average precipitation and **d–f** histogram of tropical marine precipitation for (left-to-right) aquaplanet experiments, AMIP experiments, and CESM2 cloud-locking experiments. Colors are as noted in legends, with solid curves showing the control simulations and dashed curves showing the LWoff or cloud-locked simulations.

experiments, the absence of LWCRE allows outgoing LW radiation to increase, but downwelling LW radiation at the surface decreases, while upwelling LW is (largely) unchanged; the net result is that more radiant energy enters the atmosphere, which must be balanced by a decrease in precipitation (and evaporation).

The global decrease in precipitation in the LWoff experiments is shown in Fig. 2a (open triangles for AMIP experiments and circles for aquaplanets). Separating ocean gridpoints in the Earth-like configurations (solid triangles) shows different changes, in some cases even increasing precipitation over the oceans from the control climate to the LWoff climate. Differences between the global and ocean-only changes indicate a redistribution of precipitation between land and ocean. Figure 2b shows mean tropical precipitation (30°S–30°N), which generally increases in LWoff (the exception being the CESM2 aquaplanet). There is a tendency for differences in tropical oceanic precipitation to have the same sign as the tropics-wide difference, but the oceanic changes are larger in the AMIP experiments. Notably, the change in tropical mean precipitation is not necessarily related to the change in maximum zonal mean precipitation; in many cases (especially the aquaplanets), the peak zonal mean precipitation decreases, while the tropical mean increases as the tropical rain belts widen.

Turning to the extreme tail of the precipitation distribution, the lower row of Fig. 1 shows that removing LWCRE results in a reduction in extremes. Only the CNRM aquaplanet shows much resiliency to the LWoff experiment, with the 99.9th percentile of tropical oceanic precipitation (shown by dots) hardly changing from the control. Figure 1d–f focus on tropical ocean locations where most extreme precipitation occurs in all the models (not shown, but consistent with observations, e.g., ref. [30]). Figure 2c shows the 95th percentile of the tropical ocean daily precipitation rate (P_{95}) for each simulation; most of the simulations show a slight reduction in P_{95}, while two AMIP experiments (CESM2 and CNRM) show increases. Comparing with the histograms in Fig. 1, the discrepancy is understood by the models manifesting differing changes in the shape of the distribution tail; that is, for any particular model, the change in the extreme precipitation is not a simple scaling applied to the control climate's precipitation distribution. To better account for this nonlinear response, we apply a simple metric to understand how the extreme precipitation changes: define the extreme fraction as the total precipitation falling at or greater than the 95th percentile precipitation rate divided by the total accumulated precipitation ($\varphi = (\sum_{P_{95}}^{\infty} P)/(\sum_{0}^{\infty} P)$). This metric is shown in Fig. 2d; every experiment shows a weakening of the extreme fraction when LWCRE is removed, but there is a spread of magnitudes of the change.

Cloud-locking experiments

While the COOKIE methodology allows us to compare across models, it also alters the mean climatic state by removing a substantial atmospheric heat source[36]. The impact on the mean is demonstrated, for example, by the global mean precipitation changes because of the change in radiative cooling of the system (Table 1). Changes in the mean state are often thought to impact aspects of the atmosphere that could influence extreme precipitation. For instance, the MJO, which helps to organize convection in the tropics, is sensitive to the background state [44–46]. One might wonder whether the changes in the mean state are responsible directly or indirectly for the change in extreme precipitation.

To address this potential confounding effect, additional experimental designs are needed that remove CREs without dramatically altering the mean state. In limited-domain CRM experiments, one approach is to homogenize the CRE at each time step, spreading the heating across the domain[18]. That approach is inappropriate for global models because of the wider range of meteorological regimes. Another approach is to lock the CREs by providing cloud fields to the radiative transfer calculation that are

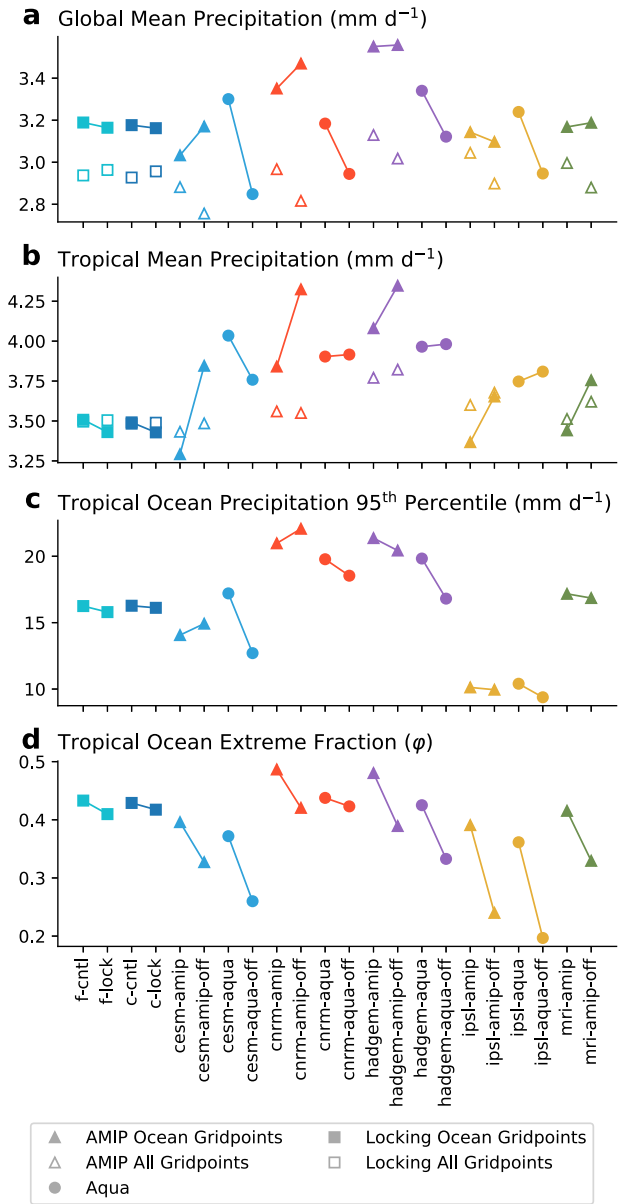

Fig. 2 Summary statistics from the experiments. Lines connect pairs of simulations to highlight the changes over oceans. Panels **a** and **b** separately show ocean gridpoints (filled markers) and all gridpoints (open markers). Colors denote models as in Fig. 1.

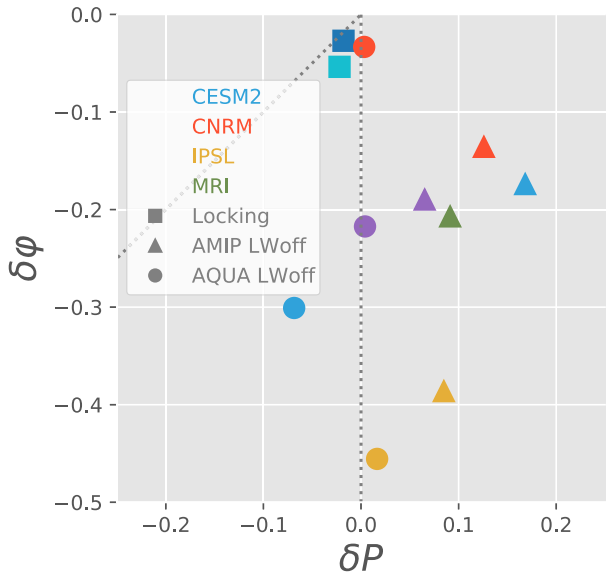

Fig. 3 The fractional change in extreme precipitation fraction ($\delta\varphi$) against tropical ocean mean precipitation (δP). Dashed diagonal line in the upper left shows the one-to-one line, and a vertical line at $\delta P = 0$.

independent of the flow field. By using cloud fields from a separate simulation with a given model, this approach has been shown to maintain the mean climate very well[8,12,47,48]. The approach maintains the spatial, seasonal, and diurnal structure of CRE, but instantaneously removes the correlation between the atmospheric state and the clouds as seen by the radiative transfer.

The cloud-locking approach has been applied to CESM2 in both coupled and prescribed-SST configurations. The simulations have been described in detail in previous studies[12,48]; we denote them using *c* (coupled) and *f* (fixed SST) modifying either "control" or "lock". Relevant to the present application, it has been shown that cloud-radiative feedbacks alter tropical variability[12]. We extend that analysis by considering the impact of cloud-radiative feedbacks on extreme precipitation. Consistent with the previous analysis, the mean precipitation globally and tropically appears to change only slightly between the control and cloud-locked climates (Figs. 1c and 2, square markers). The differences are generally smaller than in the LWoff experiments. Both Figs. 1 and 2 suggest that the coupled and fixed-SST configurations produce nearly identical climates (by construction; the fixed-SST simulation uses monthly SST from the coupled simulation). Extreme precipitation reduces, although modestly compared to the LWoff experiments. The fraction of precipitation that is extreme reduces when CRE is locked, although again the reduction is muted compared to most of the LWoff experiments.

Figure 3 shows the fractional change in extreme precipitation plotted against the fractional change in mean precipitation, both over tropical oceans. The cloud-locking experiments show slight reductions in both mean and extreme precipitation, but the reduction in an extreme fraction is larger than the reduction in mean precipitation. Bootstrapped significance testing (not shown) indicates that this difference is significant with >95% confidence. All the LWoff experiments show reduced extreme precipitation. The tropical oceanic mean precipitation increases in the AMIP-LWoff experiments, and shows small changes in the aquaplanets. Figure 3 does not support a connection between the response of the mean precipitation and the extreme precipitation.

The muted response in the cloud-locking experiments with CESM2 compared to the LWoff experiments indicates that feedbacks in LWoff experiments enhance the response of extreme precipitation. The cloud-locking methodology specifies the mean CRE (including preserving seasonal and diurnal cycles), which provides a constraint on the atmospheric state. The LWoff methodology, on the other hand, removes CRE altogether along with all feedbacks that involve CRE, thus allowing the model state to adjust to LWoff conditions much more strongly than cloud-locked conditions. In some ways, this comparison is like that between the aquaplanet and the AMIP-LWoff experiments, where we inferred that additional variability in the more geographically realistic AMIP configuration reduces the effect of eliminating CRE. Here, we deduce that the LWoff methodology allows an amplification of the response by allowing the mean state to adjust, while cloud-locking focuses on the nearly instantaneous consequence of removing the feedback between CRE and the atmospheric state. The large difference between the CESM2 cloud-locking and LWoff results shows that CREs are crucial for determining the tropical climate.

The weakening of extreme precipitation in the cloud-locking experiments (Fig. 1f) in excess of the change in the mean precipitation (Fig. 3) bolsters evidence from the LWoff experiments that there is a causal relationship between CRE and extreme precipitation. This result, which has not been previously demonstrated in climate models, indicates the potential for model biases in cloud-radiative properties to influence the representation of extreme events. Deficiencies in representing clouds have long been known to contribute to uncertainty in climate sensitivity[49,50], and this result suggests that clouds may also contribute to uncertainty in projections of climate extremes.

DISCUSSION

We have found that CREs act to increase the probability of extreme tropical precipitation. This finding holds across several climate models in both idealized aquaplanet and more realistic AMIP configurations. We have also re-examined previous COOKIE experiments with different models that removed both SWCRE and LWCRE in aquaplanet and AMIP configurations and find similar changes (not shown), consistent with other studies of those experiments[6,11,39]. The result also holds for CESM2 cloud-locking experiments that preserve the mean state.

The robustness of this finding seems somewhat at odds with studies reporting a diversity of biases and climate responses of extreme precipitation in climate models[33,51–53]. With warming, global mean precipitation increases, and extreme precipitation usually increases, but varies among models. An example is shown in Fig. 4a for the case of a uniform 4K SST warming in both AMIP and aquaplanet configurations. While the tropical ocean mean precipitation increases by 10–20% (or 2.5–5%; K^{-1}, consistent with other studies[54]), the extreme precipitation fraction changes are <10% and vary in sign among the models.

Repeating the uniform warming experiment in LWoff configurations also shows an increase in mean precipitation and mixed results for extreme precipitation fraction (Fig. 4c). Without LWCRE, the responses to warming are slightly more similar across models, but the qualitative similarity of Fig. 4a and 4c suggests that the precipitation response to warming is not dominated by cloud-radiative feedbacks. Performing the complementary comparison, the precipitation changes that occur when LWCRE is removed from the warmer climate (i.e., the uniform 4K SST increase) are similar to the cooler climate (Fig. 4d is similar to Fig. 3).

For a warming climate, several mechanisms could impact the extreme end of the precipitation distribution[55,56]. These can be briefly stated as changes in atmospheric moisture, atmospheric stability, or changes that are related to the distribution of convective motions. These same mechanisms are candidates to understand the role of CRE in extreme precipitation, so we consider each.

Altered atmospheric moisture content—absent circulation changes—would impact both extreme and moderate precipitation. A more humid atmosphere tends to rain more; for example, rain increases in the tropics as the column approaches saturation[57]. There is a modest reduction in vertically integrated water vapor in the tropics in the LWoff simulations, but as seen in Fig. 3, the mean precipitation does not consistently change. Furthermore, the difference in atmospheric moisture in the CESM2 cloud-locking experiments is not significant (using Welch's two-tailed *t* test). A simple response to moisture content, therefore, seems unlikely. Not only that, but the circulation and the convection that produce extreme precipitation interact, and the assumption that circulation does not change is unlikely to be valid, and clearly is not the case in the aquaplanet experiments (Fig. 1).

Another potential mechanism to reduce extreme precipitation is to enhance atmospheric stability. When stability increases, convection is inhibited: weakening the strongest convection could weaken precipitation extremes. Examination of the differences in the temperature lapse rate in LWoff experiments (not shown) indicates that stability increases in the tropical tropopause layer (TTL), but decreases through the troposphere. This may indicate that clouds act to stabilize the troposphere and inhibit weak convection while destabilizing the TTL, allowing strong convection to reach higher. Atmospheric CO_2-quadrupling simulations provide a direct test for the impact of increasing stability. In these experiments, the atmospheric CO_2 is increased with no other changes (in particular, the sea-surface temperature is the same as in the corresponding control simulation). The effect of increasing CO_2 is to make the atmosphere optically thicker, raising the effective emission level, warming and stabilizing the atmosphere (the stabilizing effect is strongest in the TTL, similar to the LWoff experiments). Taking the same set of models as in Fig. 1 and examining the precipitation changes under this increased stability, we find, in general, a slight *increase* in the extreme fraction along with the expected decrease in the mean precipitation (Fig. 4b). Stabilizing the TTL, therefore, does not directly control extreme precipitation. The cloud-locking experiments have no change in time-mean stability, so it is unlikely that changes in mean stability are primarily responsible for weakening extreme precipitation in LWoff simulations. The impact of CRE on tropospheric stability, however, may contribute to the larger changes in extreme precipitation in the LWoff experiments compared to cloud-locking experiments.

Latent heat release within convective clouds helps to provide buoyancy in rising plumes, providing additional strength to storms. In the LWoff experiments, however, latent heating is not directly changed, so is not a viable causal effect on the weakening extreme precipitation. It is worth noting, however, that vertical velocity weakens at gridpoints with extreme precipitation in LWoff simulations, suggesting that the reduced precipitation intensity is linked to the strength of convection.

Although latent heating is the primary source of energy for growing convective clouds, radiative heating could similarly reinforce convection. The connection between radiative heating and tropical anvil clouds has been investigated in models and observations, but usually on scales unresolved by climate models. Such studies indicate that LW radiative heating occurs at the base of anvil clouds, while radiative cooling occurs at the top, destabilizing the cloud layer. Shortwave radiative heating counteracts this destabilization during the daytime[58]. The radiative effects of clouds might also foster secondary circulations by promoting horizontal gradients between cloudy and clear regions[59,60]. While climate models do not explicitly represent such small-scale cloud dynamics, they do roughly capture the diurnal cycle of convection and precipitation over the tropical oceans[61], so some aspects of cloud-radiation interactions observed for anvil clouds are likely to be captured as well. Moreover, the climate models can produce clusters of convection that might mimic MCSs, where similar mechanisms have been examined[62,63].

Since much of the tropical extreme precipitation falls in mesoscale systems[29], and since large-scale changes in the environment do not seem to account for the response of extreme precipitation to changes in CRE, we have also examined some aspects of organized convection across these models.

Figure 5 shows a summary of changes to propagating equatorial wave variability resulting from deactivating CRE in the AMIP and aquaplanet LWoff experiments. Color shading shows the percent change of the non-normalized spectral power of the tropical precipitation component symmetric about the equator[64,65]. Disabling CRE generally weakens disturbances within the so-called moisture mode group of tropical systems: tropical depression-like waves, equatorial Rossby waves, and the MJO[66]. These phenomena are the dominant drivers of extreme precipitation in the tropics and subtropics[67,68]. At the same time, gravity waves (Kelvin waves and inertial gravity waves) are enhanced (or less suppressed) compared to moisture modes. The shifts in

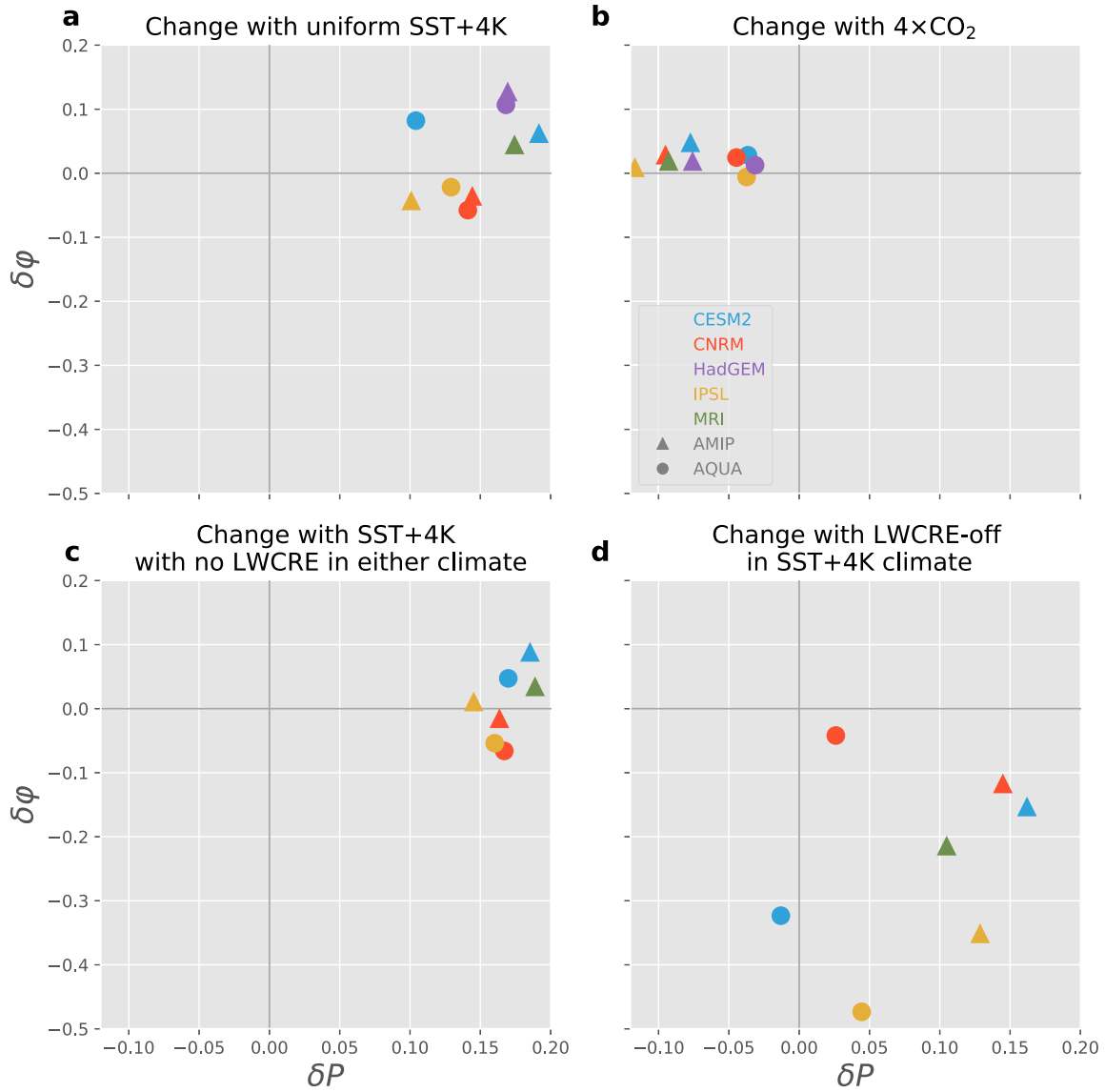

Fig. 4 Fractional changes in extreme precipitation fraction (δφ) and tropical ocean mean precipitation (δP) for additional experiments. As in Fig. 3 but for **a** changes with uniform 4K SST warming (*amip-p4K* minus *amip*), **b** the response to a quadrupling of atmospheric CO_2 with unchanged prescribed-SST (*amip-4* × CO_2 minus *amip*), **c** changes with uniform warming between the LWoff simulations (*amip-p4K-lwoff* minus *amip-lwoff*), and **d** changes when LWCRE is removed in a warmer climate (i.e., as in Fig. 3, but with a warmer reference climate, *amip-p4K-lwoff* minus *amip-p4K*). Italics denote CMIP experiment names, using the AMIP names (aquaplanets follow a similar pattern).

tropical wave activity when CRE are removed agree with cloud-locking experiments with CESM2[12]. In that case, the MJO weakening was connected to suppressed radiation-convection positive feedbacks and increased gross moist stability. The IPSL model is the sole exception; that model deviates most from the observed tropical wave spectrum (not shown here) in having very weak wave activity, and produces a dramatic reduction of tropical precipitation variability that is uniform across spectral space in the LWoff simulations.

Another view of organized convection in these experiments can be discerned by detecting and tracking extreme precipitation events. We have applied a simple algorithm that identifies as events connected gridpoints (in space or time) that have daily precipitation greater than or equal to that simulation's tropical oceanic 99th percentile[34]. The detected events do not necessarily align with propagating waves detected by the spectral analysis because rapidly propagating systems are unlikely to meet the temporal overlap condition and because propagating waves modulate precipitation across intensities. The detected extreme events, on the other hand, capture all extreme precipitation by construction.

Figure 6 summarizes the number, duration, and size of these precipitation events over tropical oceans. When cloud-radiative feedbacks are removed, most of the experiments show a decrease in the number of identified extreme events. Most extreme events are identified only in one day (the smallest possible increment since we use daily mean precipitation), making the median duration the same (identically one) in all simulations. Removing the smallest events (those with a duration of <2 days or size < 2 gridpoints) results in an increase in duration to 4 days, with an interquartile range that varies slightly across simulations. Evidently, the distribution of event duration is so dominated by short events that it is difficult to discern differences. The size of events (defined here as the fraction of tropical oceanic gridpoints occupied by each event) shows some sensitivity to cloud-radiative feedbacks. Specifically, events (again excluding the smallest events, shown by the colored

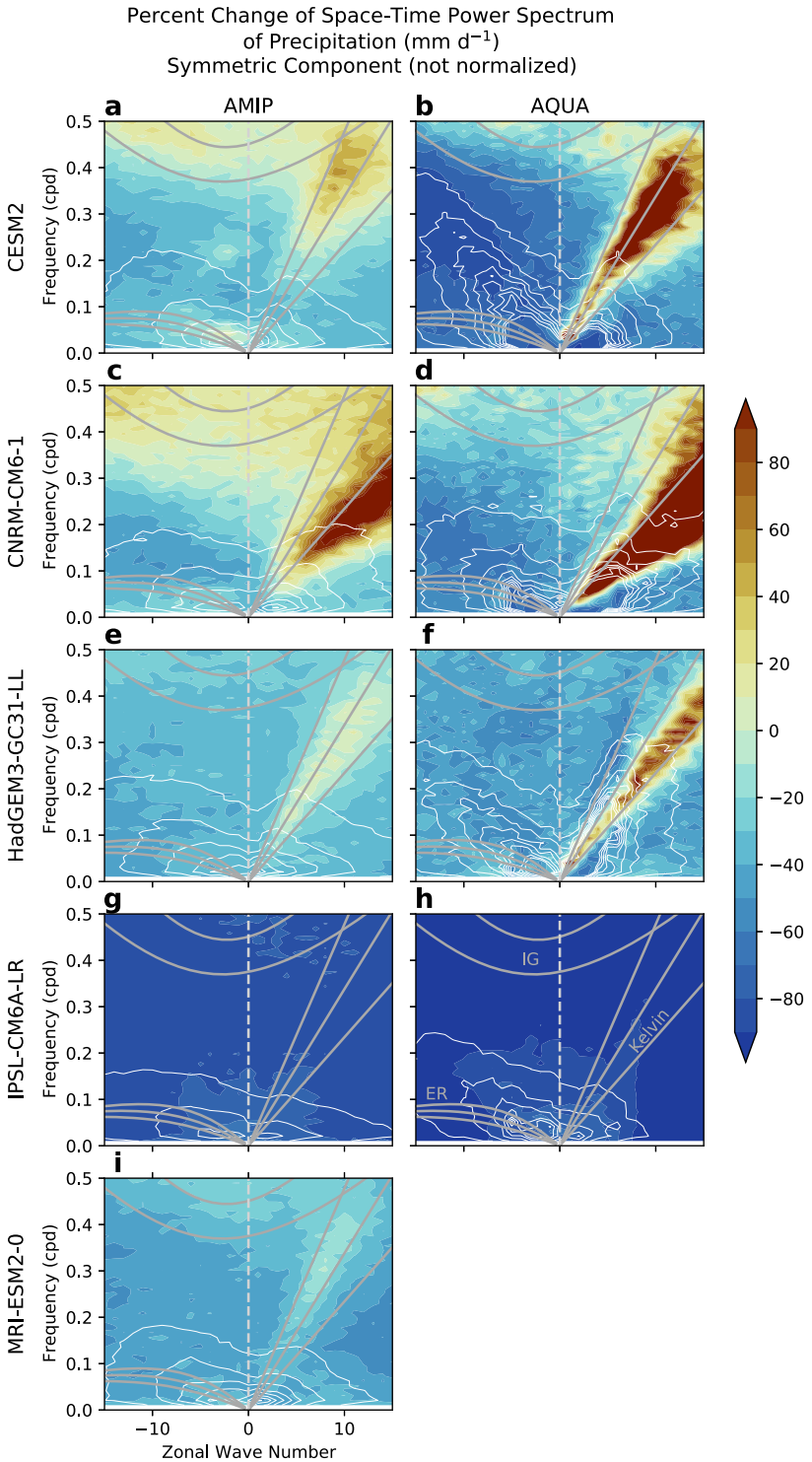

Fig. 5 Changes in wavenumber-frequency power spectra with LWoff. Color shading in each panel shows the percent difference, expressed as 100 × (LWoff − control)/control, of the non-normalized zonal wavenumber-frequency power spectra for the precipitation component symmetric about the equator for each model simulation. White contours show the associated spectral power using log base-10 scaling from the associated control simulation as a reference (contour interval is 0.15 up to 1.2). Powers are summed over 15°S–15°N. Thick gray lines indicate shallow water dispersion curves for equivalent depths of 12, 25, and 50 m, annotations in panel **h** indicate Kelvin, equatorial Rossby (ER), and inertial gravity (IG) waves.

markers) tend to be slightly larger in LWoff simulations than in control simulations; this also holds for the cloud-locking experiments. Only two experiments show a different response: the CESM2 aquaplanet and the MRI AMIP experiments. These are the same two experiments that show an increase in the number of events.

While suggestive, the detected extreme events should be viewed with some skepticism. Using daily mean precipitation may obscure higher frequency structure, removing some short but intense storms and blurring multiple events over consecutive days into long-lasting events. Sensitivity tests of the detection and

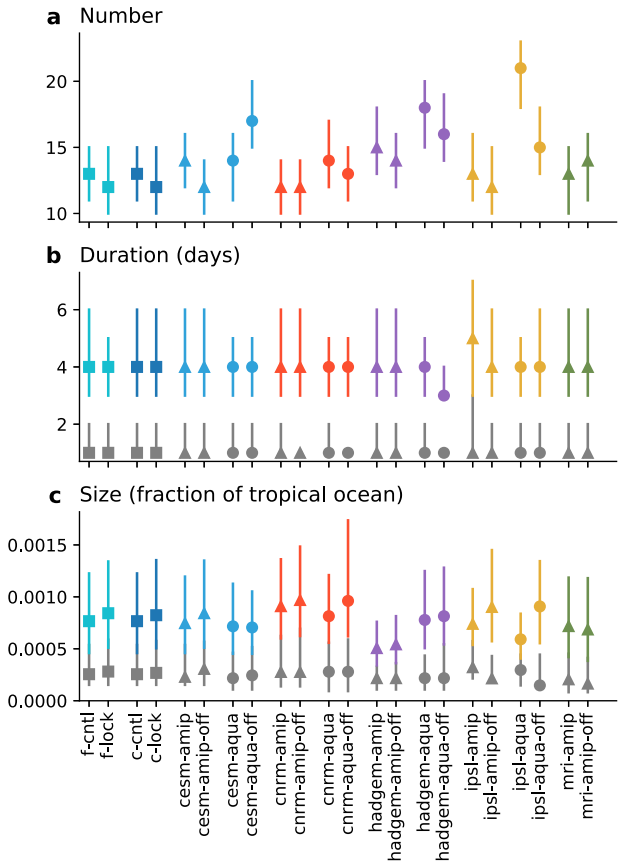

Fig. 6 Summary of extreme tropical ocean precipitation events. **a** Median number, **b** median duration, and **c** median size. Gray markers show the median duration and size of all events, while colors in those panels exclude events that are shorter than 2 days or smaller than 2 grid cells; colors indicate model, as in other figures. Error bars show the interquartile range. The simulations are paired into experiments horizontally.

tracking method showed that parameter choices, such as the thresholds used, the region analyzed, and assumptions about temporal connectivity, can impact statistics. Other tracking methods have similar sensitivities[69]. Many events are short and/or small, and could be interpreted as "gridpoint storms" that are dominated by resolved ascending motion and stratiform processes; the veracity of such storms in climate models has sometimes been called into question[70,71]. Many detected events, however, are long-lived and relatively large, and are reminiscent of real phenomena like tropical depressions.

On the whole, these results give the impression that aspects of organized convection depend on cloud-radiative feedbacks. Propagating waves appear to be impacted, with moisture modes especially suppressed without cloud-radiative feedbacks. Individual convective events generally become less common, but larger when cloud-radiative feedbacks are removed. Two experiments in different models show the opposite response. Convective event statistics could change in LWoff experiments because of parameter choices, but may also depend on changes in the mean state (that would in turn interact with cloud-radiative feedbacks).

These results are consistent with the arguments using extreme precipitation scaling[33,34]. Extreme precipitation scales like the vertically integrated condensation, which is related to the vertical transport of saturation specific humidity along pseudo-adiabats. In those analyses, the scaling is applied to data with extreme precipitation (e.g., $P > P_{99}$). A finding from such analysis is that vertical velocity is a key contributor to extreme precipitation changes in climate change experiments. As noted above, we have examined the vertical velocity conditioned on $P > P_{99}$ (and also $P > P_{95}$) in the LWoff and cloud-locking experiments, and in all cases, we find weaker upward velocity without cloud-radiative feedbacks (not shown). Extreme precipitation scaling can be decomposed into dynamic, thermodynamic, and microphysical contributions. Our results may indicate that CRE affect precipitation extremes by influencing the organization of convection, consistent with a dynamic effect. It is plausible that CRE impact the microphysical contribution as well by enhancing convective organization and exerting an influence on precipitation efficiency. We have not attempted to disentangle these effects.

In summary, this study has shown that cloud-radiative feedbacks enhance extreme precipitation over the tropical oceans. The impact is robust across a hierarchy of climate model experiments from idealized aquaplanets to realistic configurations driven by prescribed sea-surface temperature to coupled cloud-locking experiments. In all cases, the reduction in the extreme tail of the precipitation distribution is more negative than the change in the tropical mean precipitation, which sometimes even increases when cloud-radiative feedbacks are removed. There is a tendency for the reduction of extremes to be smaller in experiments with realistic geography than in aquaplanets, and smaller yet in the cloud-locking experiments. This tendency shows that there are other aspects of the system that also impact extreme precipitation (e.g., interannual variability, stationary waves, etc.). The smaller effect with cloud-locking, in particular, indicates that CREs amplify convection and extreme precipitation on short timescales and trigger positive feedbacks between CRE and the convective atmosphere. The fact that extreme precipitation is impacted by cloud-radiative feedbacks implies that errors in the representation of clouds could play into biases in the hydrologic cycle, including high-impact events such as atmospheric rivers and tropical cyclones.

The interaction between CREs and extreme precipitation does not appear to be closely related to the relationship between clouds and the mean state. Increasing the tropospheric stability with a quadrupling of CO_2 leads to increased precipitation extremes. Warming the system by uniformly increasing the sea-surface temperature shows mixed results in extreme precipitation, despite increased atmospheric water vapor. The connection appears to be more closely related to aspects of organized convection, evidenced by tendencies for suppressed moisture modes as well as fewer but larger precipitating systems.

The CFMIP archive provides a limited number of models with these experiments, and with limited model output saved to explore particular mechanisms. A more detailed study of processes involved may require dedicated experiments with more focused, high-frequency output. The results shown here, however, provide strong evidence that cloud-radiative feedbacks strengthen extreme precipitation. This finding has not been identified previously in climate models. Our analysis also supports the hypothesis that this connection is mediated by the representation of organized convection. Future work should deepen the understanding of the impact of cloud-radiative feedbacks on organized convection and the physics of extreme precipitation, including the relative roles of vertical velocity and cloud microphysics. Current climate models inadequately resolve tropical convective systems, and it will be interesting to see how CREs impact the precipitation distribution at a higher resolution. Establishing the connection between cloud-radiative feedbacks and extreme precipitation may also help to better understand the changing climate as both clouds and precipitation respond to forcing and influence one another.

DATA AVAILABILITY

The CMIP data are publicly available via the Earth System Grid Federation, which can be accessed at https://esgf-node.llnl.gov/search/cmip6/. The CESM2 cloud-locking experiment data sets are archived at https://www.zenodo.org (https://doi.org/10.5281/zenodo.3591996).

CODE AVAILABILITY

Analysis codes to produce the figures are available at https://github.com/brianpm/cre_pex or by contacting the corresponding author. Code to implement cloud locking in CESM2 is also available from the corresponding author.

Received: 20 November 2020; Accepted: 18 February 2021;
Published online: 17 March 2021

REFERENCES

1. Loeb, N. G. et al. Clouds and the earth's radiant energy system (CERES) energy balanced and filled (EBAF) top-of-atmosphere (TOA) edition-4.0 data product. *J. Clim.* **31**, 895–918 (2018).
2. Shupe, M. D. & Intrieri, J. M. Cloud radiative forcing of the Arctic surface: the influence of cloud properties, surface albedo, and solar zenith angle. *J. Clim.* **17**, 616–628 (2004).
3. Allan, R. P. Combining satellite data and models to estimate cloud radiative effect at the surface and in the atmosphere. *Meteorol. Appl.* **18**, 324–333 (2011).
4. Li, Y., Thompson, D. W. J. & Bony, S. The influence of atmospheric cloud radiative effects on the large-scale atmospheric circulation. *J. Clim.* **28**, 7263–7278 (2015).
5. Wild, M. The global energy balance as represented in CMIP6 climate models. *Clim. Dyn.* **55**, 553–577 (2020).
6. Fermepin, S. & Bony, S. Influence of low-cloud radiative effects on tropical circulation and precipitation. *J. Adv. Model. Earth Syst.* **6**, 513–526 (2014).
7. Radel, G. et al. Amplification of El Nino by cloud longwave coupling to atmospheric circulation. *Nat. Geosci.* **9**, 106–110 (2016).
8. Middlemas, E. A., Clement, A. C., Medeiros, B. & Kirtman, B. Cloud radiative feedbacks and El Niño–Southern Oscillation. *J. Clim.* **32**, 4661–4680 (2019).
9. Kolly, A. & Huang, Y. The radiative feedback during the ENSO cycle: observations versus models. *J. Geophys. Res. Atmos.* **123**, 9097–9108 (2018).
10. Middlemas, E., Clement, A. & Medeiros, B. Contributions of atmospheric and oceanic feedbacks to subtropical northeastern sea surface temperature variability. *Clim. Dyn.* **53**, 6877–6890 (2019).
11. Crueger, T. & Stevens, B. The effect of atmospheric radiative heating by clouds on the Madden-Julian oscillation. *J. Adv. Model. Earth Syst.* **7**, 854–864 (2015).
12. Benedict, J. J., Medeiros, B., Clement, A. C. & Olson, J. G. Investigating the role of cloud-radiation interactions in subseasonal tropical disturbances. *Geophys. Res. Lett.* **47**, e2019GL086817 (2020).
13. Del Genio, A. D. & Chen, Y. Cloud-radiative driving of the Madden-Julian oscillation as seen by the A-Train. *J. Geophys. Res. Atmos.* **120**, 5344–5356 (2015).
14. Bu, Y. P., Fovell, R. G. & Corbosiero, K. L. Influence of cloud–radiative forcing on tropical cyclone structure. *J. Atmos. Sci.* **71**, 1644–1662 (2014).
15. Ruppert, J. H., Wing, A. A., Tang, X. & Duran, E. L. The critical role of cloud-infrared radiation feedback in tropical cyclone development. *Proc. Natl. Acad. Sci.* **117**, 27884–27892 (2020).
16. Zhang, B., Soden, B. J., Vecchi, G. A. & Yang, W. The role of radiative interactions in tropical cyclone development under realistic boundary conditions. *J. Clim. 1–38* **34**, 2079–2091 (2020).
17. Stephens, G. L., van den Heever, S. & Pakula, L. Radiative–convective feedbacks in idealized states of radiative–convective equilibrium. *J. Atmos. Sci.* **65**, 3899–3916 (2008).
18. Harrop, B. E. & Hartmann, D. L. The role of cloud radiative heating within the atmosphere on the high cloud amount and top-of-atmosphere cloud radiative effect. *J. Adv. Model. Earth Syst.* **8**, 1391–1410 (2016).
19. Bretherton, C. S., Blossey, P. N. & Khairoutdinov, M. An energy-balance analysis of deep convective self-aggregation above uniform SST. *J. Atmos. Sci.* **62**, 4273–4292 (2005).
20. Popke, D., Stevens, B. & Voigt, A. Climate and climate change in a radiative-convective equilibrium version of ECHAM6. *J. Adv. Model. Earth Syst.* **5**, 1–14 (2013).
21. Reed, K. A., Medeiros, B., Bacmeister, J. T. & Lauritzen, P. H. Global radiative–convective equilibrium in the Community Atmosphere Model, Version 5. *J. Atmos. Sci.* **72**, 2183–2197 (2015).
22. Wing, A. A. et al. Clouds and convective self-aggregation in a multimodel ensemble of radiative-convective equilibrium simulations. *J. Adv. Model. Earth Syst.* **12**, e2020MS002138 (2020).
23. Coppin, D. & Bony, S. Physical mechanisms controlling the initiation of convective self-aggregation in a general circulation model. *J. Adv. Model. Earth Syst.* **7**, 2060–2078 (2015).
24. Arnold, N. P. & Randall, D. A. Global-scale convective aggregation: implications for the Madden-Julian oscillation. *J. Adv. Model. Earth Syst.* **7**, 1499–1518 (2015).
25. Nakazawa, T. Tropical super clusters within intraseasonal variations over the Western Pacific. *J. Meteorol. Soc. Jpn.* **66**, 823–839 (1988).
26. Tobin, I., Bony, S. & Roca, R. Observational evidence for relationships between the degree of aggregation of deep convection, water vapor, surface fluxes, and radiation. *J. Clim.* **25**, 6885–6904 (2012).
27. Holloway, C. E. et al. Observing convective aggregation. *Surv. Geophys.* **38**, 1199–1236 (2017).
28. Nesbitt, S. W., Cifelli, R. & Rutledge, S. A. Storm morphology and rainfall characteristics of TRMM precipitation features. *Mon. Weather Rev.* **134**, 2702–2721 (2006).
29. Tan, J., Jakob, C. & Lane, T. P. On the identification of the large-scale properties of tropical convection using cloud regimes. *J. Clim.* **26**, 6618–6632 (2013).
30. Hamada, A., Murayama, Y. & Takayabu, Y. N. Regional characteristics of extreme rainfall extracted from TRMM PR measurements. *J. Clim.* **27**, 8151–8169 (2014).
31. Tan, J., Jakob, C., Rossow, W. B. & Tselioudis, G. Increases in tropical rainfall driven by changes in frequency of organized deep convection. *Nature* **519**, 451–454 (2015).
32. Schumacher, R. S. & Johnson, R. H. Organization and environmental properties of extreme-rain-producing mesoscale convective systems. *Mon. Weather Rev.* **133**, 961–976 (2005).
33. O'Gorman, P. A. & Schneider, T. The physical basis for increases in precipitation extremes in simulations of 21st-century climate change. *Proc. Natl. Acad. Sci. USA* **106**, 14773–14777 (2009).
34. Pendergrass, A. G., Reed, K. A. & Medeiros, B. The link between extreme precipitation and convective organization in a warming climate: global radiative-convective equilibrium simulations. *Geophys. Res. Lett.* **43**, 11,445–11,452 (2016).
35. Watt-Meyer, O. & Frierson, D. M. W. Local and remote impacts of atmospheric cloud radiative effects onto the eddy-driven jet. *Geophys. Res. Lett.* **44**, 10,036–10,044 (2017).
36. Voigt, A. & Albern, N. No cookie for climate change. *Geophys. Res. Lett.* **46**, 14751–14761 (2019).
37. Webb, M. J. et al. The cloud feedback model intercomparison project (CFMIP) contribution to CMIP6. *Geosci. Model Dev.* **10**, 359–384 (2017).
38. Lau, W. K. M., Kim, K.-M., Chern, J.-D., Tao, W. K. & Leung, L. R. Structural changes and variability of the ITCZ induced by radiation–cloud–convection–circulation interactions: inferences from the Goddard Multi-scale Modeling Framework (GMMF) experiments. *Clim. Dyn.* **54**, 211–229 (2020).
39. Harrop, B. E. & Hartmann, D. L. The role of cloud radiative heating in determining the location of the ITCZ in aquaplanet simulations. *J. Clim.* **29**, 2741–2763 (2016).
40. O'Gorman, P. A., Allan, R. P., Byrne, M. P. & Previdi, M. Energetic constraints on precipitation under climate change. *Surv. Geophys.* **33**, 585–608 (2012).
41. Allen, M. R. & Ingram, W. J. Constraints on future changes in climate and the hydrologic cycle. *Nature* **419**, 228–232 (2002).
42. Mitchell, J. F. B., Wilson, C. A. & Cunnington, W. M. On CO_2 climate sensitivity and model dependence of results. *Q. J. R. Meteorol. Soc.* **113**, 293–322 (1987).
43. Pendergrass, A. G. & Hartmann, D. L. The atmospheric energy constraint on global-mean precipitation change. *J. Clim.* **27**, 757–768 (2014).
44. Slingo, J. M. et al. Intraseasonal oscillations in 15 atmospheric general circulation models: results from an AMIP diagnostic subproject. *Clim. Dyn.* **12**, 325–357 (1996).
45. Fink, A. & Speth, P. Some potential forcing mechanisms of the year-to-year variability of the tropical convection and its intraseasonal (25–70-day) variability. *Int. J. Climatol.* **17**, 1513–1534 (1997).
46. Zhang, C. & Dong, M. Seasonality in the Madden–Julian Oscillation. *J. Clim.* **17**, 3169–3180 (2004).
47. Langen, P. L., Graversen, R. G. & Mauritsen, T. Separation of contributions from radiative feedbacks to polar amplification on an aquaplanet. *J. Clim.* **25**, 3010–3024 (2012).
48. Grise, K. M., Medeiros, B., Benedict, J. J. & Olson, J. G. Investigating the influence of cloud radiative effects on the extratropical storm tracks. *Geophys. Res. Lett.* **46**, 7700–7707 (2019).
49. Sherwood, S. et al. An assessment of Earth's climate sensitivity using multiple lines of evidence. *Rev. Geophys.* e2019RG000678 (2020)..
50. Zelinka, M. D. et al. Causes of higher climate sensitivity in CMIP6 models. *Geophys. Res. Lett.* **47**, e2019GL085782 (2020).
51. Scoccimarro, E. & Gualdi, S. Heavy daily precipitation events in the CMIP6 worst-case scenario: projected twenty-first-century changes. *J. Clim.* **33**, 7631–7642 (2020).
52. Lopez-Cantu, T., Prein, A. F. & Samaras, C. Uncertainties in future U.S. extreme precipitation from downscaled climate projections. *Geophys. Res. Lett.* **47**, e2019GL086797 (2020).
53. Pendergrass, A. G. & Hartmann, D. L. Changes in the distribution of rain frequency and intensity in response to global warming. *J. Clim.* **27**, 8372–8383 (2014).

54. Held, I. M. & Soden, B. J. Robust responses of the hydrological cycle to global warming. *J. Clim.* **19**, 5686–5699 (2006).
55. Pendergrass, A. G. & Gerber, E. P. The rain is askew: two idealized models relating vertical velocity and precipitation distributions in a warming world. *J. Clim.* **29**, 6445–6462 (2016).
56. Pendergrass, A. G. What precipitation is extreme? *Science* **360**, 1072–1073 (2018).
57. Bretherton, C. S., Peters, M. E. & Back, L. E. Relationships between water vapor path and precipitation over the tropical oceans. *J. Clim.* **17**, 1517 – 1528 (2004).
58. Wall, C. J. et al. Observational evidence that radiative heating modifies the life cycle of tropical anvil clouds. *J. Clim.* **33**, 8621–8640 (2020).
59. Lilly, D. K. Cirrus outflow dynamics. *J. Atmos. Sci.* **45**, 1594–1605 (1988).
60. Schmidt, C. T. & Garrett, T. J. A simple framework for the dynamic response of cirrus clouds to local diabatic radiative heating. *J. Atmos. Sci.* **70**, 1409–1422 (2013).
61. Covey, C. et al. Metrics for the diurnal cycle of precipitation: toward routine benchmarks for climate models. *J. Clim.* **29**, 4461–4471 (2016).
62. Miller, R. A. & Frank, W. M. Radiative forcing of simulated tropical cloud clusters. *Mon. Weather Rev.* **121**, 482–498 (1993).
63. Xu, K.-M. & Randall, D. A. Impact of interactive radiative transfer on the macroscopic behavior of cumulus ensembles. Part II: mechanisms for cloud-radiation interactions. *J. Atmos. Sci.* **52**, 800–817 (1995).
64. Wheeler, M. & Kiladis, G. N. Convectively coupled equatorial waves: analysis of clouds and temperature in the wavenumber–frequency domain. *J. Atmos. Sci.* **56**, 374–399 (1999).
65. Kiladis, G. N., Wheeler, M. C., Haertel, P. T., Straub, K. H. & Roundy, P. E. Convectively coupled equatorial waves. *Rev. Geophys*. **47,** 2008RG000266 (2009). https://doi.org/10.1029/2008RG000266.
66. Adames, Á. F., Kim, D., Clark, S. K., Ming, Y. & Inoue, K. Scale analysis of moist thermodynamics in a simple model and the relationship between moisture modes and gravity waves. *J. Atmos. Sci.* **76**, 3863–3881 (2019).
67. Jones, C., Waliser, D. E., Lau, K. M. & Stern, W. Global occurrences of extreme precipitation and the Madden–Julian oscillation: observations and predictability. *J. Clim.* **17**, 4575–4589 (2004).
68. Khouakhi, A., Villarini, G. & Vecchi, G. A. Contribution of tropical cyclones to rainfall at the global scale. *J. Clim.* **30**, 359–372 (2016).
69. Zarzycki, C. M. & Ullrich, P. A. Assessing sensitivities in algorithmic detection of tropical cyclones in climate data. *Geophys. Res. Lett.* **44**, 1141–1149 (2017).
70. Held, I. M., Zhao, M. & Wyman, B. Dynamic radiative-convective equilibria using GCM column physics. *J. Atmos. Sci.* **64**, 228–238 (2007).
71. Williamson, D. L. The effect of time steps and time-scales on parametrization suites. *Q. J. R. Meteorol. Soc.* **139**, 548–560 (2013).

ACKNOWLEDGEMENTS

This material is based on work supported by the National Center for Atmospheric Research, which is a major facility sponsored by the National Science Foundation (NSF) under the Cooperative Agreement 1852977. Portions of this study were supported by the Regional and Global Model Analysis component of the Earth and Environmental System Modeling Program of the US Department of Energy's (DOE) Office of Biological and Environmental Research via NSF IA 1844590; DOE subcontract B631711; NASA PMM grant 80NSSC19K0717; and NSF Award AGS-1650209. We acknowledge the World Climate Research Program's Working Group on Coupled Modeling, which is responsible for CMIP, and we thank the climate modeling groups for producing and making available their model output. We acknowledge high-performance computing support from Cheyenne (doi:10.5065/D6RX99HX) provided by NCAR's Computational and Information Systems Laboratory, sponsored by the National Science Foundation.

AUTHOR CONTRIBUTIONS

All authors conceived the research, interpreted results, and revised the text. B.M. wrote the paper and conducted the final analyses. J.J.B. conducted the cloud-locking experiments. J.J.B. and B.Z. provided preliminary analysis that motivated the study.

COMPETING INTERESTS

The authors declare no competing interests.

ADDITIONAL INFORMATION

Correspondence and requests for materials should be addressed to B.M.

Reprints and permission information is available at http://www.nature.com/reprints

Publisher's note Springer Nature remains neutral with regard to jurisdictional claims in published maps and institutional affiliations.